Vortex pinning properties at dc and microwave frequencies of $YBa_2Cu_3O_{7-x}$ films with nanorods and nanoparticles

E. Bartolomé[1], J. Alcalà[2], F. Vallès[2], T. Puig[2], X. Obradors[2], N. Pompeo[3], A. Alimenti[3], K. Torokhtii[3], F. Rizzo[4], A. Augieri[4], G. Celentano[4], E. Silva[3], A. Palau[2]

[1] Escola Universitaria Salesiana de Sarrià (EUSS), Passeig Sant Joan Bosco 74, 08017-Barcelona, Spain
[2] Institut de Ciència de Materials de Barcelona-CSIC, Campus UAB, 08193-Bellaterra, Spain
[3] Dipartimento di Ingegneria, Università Roma Tre, Via Vito Volterra 62, 00146, Roma, Italy
[4] ENEA, Frascati Research Centre, Via E. Fermi, 45-00044 Frascati, Italy.

E-mail: palau@icmab.es

Received xxxxxx
Accepted for publication xxxxxx
Published xxxxxx

Abstract

$YBa_2Cu_3O_{7-x}$ (YBCO) nanocomposites for wire applications need to operate in a broad range of frequencies, ranging from dc in magnets to GHz in cavities and screenings of future particle accelerators. We have investigated the in-field and angular vortex pinning performance in dc and at 50 GHz of two types of nanocomposites, pulsed laser deposition (PLD) YBCO with mixed Ba_2YNbO_6 + Ba_2YTaO_6 (BYNTO) nanorods and chemical solution deposited (CSD) YBCO with $BaHfO_3$ (BHO) nanoparticles (NPs), and the pristine counterpart films, grown on top of single-crystalline substrates. Transport measurements performed up to 9 T between 5-77 K show that CSD nanocomposites exhibit a smooth field decay and increased single-to-collective crossover field H^* compared to pristine samples, associated to the enhanced isotropic pinning contribution induced by the NPs, while PLD films exhibit unchanged H^* and superior critical current densities up to higher irreversibility fields, associated to the anisotropic contribution introduced by the rods. Microwave in-field measurements of the pinning constant k_p revealed CSD NCs exhibit a qualitatively similar, but smoother $k_p(H)$ than pristine samples, whereas for PLD samples, a growing $k_p(H)$ dependence is observed as a result of the increased relevance of the stiffness of the fluxons pinned by nanorods.

Keywords: YBCO superconductor; critical current density; flux pinning; microwave measurements; nanostructured films

---

Received 3 December 2019
Accepted 30 April 2020
Published 2 June 2020

This article has been accepted for publication in IOP-Superconductor Science and Technology. This is the author's version which has not been fully edited and content may change prior to final publication.
Citation information: DOI 10.1088/1361-6668/ab8f18

1. Introduction

The outstanding ability of $YBa_2Cu_3O_{7-x}$ (YBCO) to carry high critical currents up to high magnetic fields has made it one of the most promising materials for high T_c superconducting (HTS) wires, based on second generation coated conductors, for power applications and magnets [1–5]. Moreover, in recent years high frequency applications are gaining interest, stimulated by increasing performing demands of accelerating cavities [6], and emerging fields like the hunt for galactic axions [7] or electromagnetic screenings in the future implementation of particle colliders [8–10].

With the aim of pushing the current performances under high magnetic fields as required for applications, numerous efforts have been made in the last decade towards nanoengineering the defect landscape of YBCO by introducing artificial vortex pinning centres [11–16]. Different strategies have been proposed to introduce nanodefects in YBCO thin-films grown by various methods. One of the most successful approaches has been the inclusion of non-superconducting secondary phases [17].

In particular, for vacuum-based growth techniques such as pulsed laser deposition (PLD), chemical vapour deposition (CVD), or hybrid liquid phase epitaxy (HLPE), the *in situ*, simultaneous growth of the YBCO superconductor and the secondary phases can be controlled to form self-assembled nanostructures, such as columnar nanorods along the *c*-axis, with coherent or semi-coherent interfaces with the YBCO matrix [2,11,12]. Recently, excellent magnetic flux pinning at 77 K with remarkably high irreversibility fields >10 T were achieved for PLD-grown YBCO films with YBa_2NbO_6 (YBNO or BYNO) [18], Ba_2YTaO_6 (BYTO) and mixed BYNO + BYTO (BYNTO) nanorods [19],[20].

Chemical solution deposition (CSD) routes, on the other hand, have progressed towards cost-effective production of YBCO films for applications [21–25]. In the past years, a strong effort has been devoted to prepare CSD-based YBCO nanocomposite thin-films with a variety of nanoparticle compositions (e.g. $BaZrO_3$, Ba_2YTaO_6, Y_2O_3, $BaCeO_3$, $BaSnO_3$, $BaHfO_3$ (BHO)), prepared either by the *in situ* spontaneous segregation of nanometric oxide secondary phases during the YBCO conversion [26–29], or alternatively, by the more versatile method of adding preformed nanoparticles from colloidal solutions [30–35]. It has been demonstrated that the inclusion of nanoparticles (NPs) substantially modifies the $YBa_2Cu_4O_8$ (Y124) intergrowth landscape [34,36] resulting in an increase of the nanocomposite nanostrain (ε). These nanocomposites present an enhancement of the isotropic contribution to pinning over a broad field and temperature region [15,16,37], even close to the irreversibility line [38,39].

The broad range of frequencies at which HTS wires need to operate in the various applications (from dc in magnets to GHz in cavities), requires the characterization of the nanostructured films under different dynamic vortex regimes. Ac susceptibility measurements have been used to provide insights into the vortex dynamics of YBCO nanocomposites [40] in various regimes, from high [41] to low ac amplitudes [42], at frequencies up to 10 kHz. On the other hand, surface impedance measurements at microwave (MW) frequencies (at ca. 50 GHz) have been utilized to study the response of YBCO films with different types of nano-inclusions [43–45] and CCs [46] in the regime of vortices rapidly shaking within their pinning wells. MW measurements allow to extract information [47] about the depinning frequency ν_p, the flux-flow resistivity ρ_{ff}, the pinning constant k_p, as well as to disentangle the intrinsic and effective anisotropies of the nanostructured films [48–50].

In this work, we report on the in-field vortex pinning properties of PLD and CSD nanocomposites over different frequency ranges, in the regime of long-range vortex displacements using dc resistive transport measurements, and in the regime of short-range vortex oscillations at microwave frequencies. The nanocomposites analysed were selected from those showing the best pinning performances at present, consisting on PLD-grown thin-films nanostructured with BYNTO nanorods and CSD-grown nanocomposites with embedded BHO NPs. We compare the flux pinning properties of pristine and nanocomposite PLD and CSD films at different applied magnetic field and temperatures and discuss on the better performances achieved at different operating conditions.

2. Experimental methods

CSD epitaxial *c*-axis-oriented YBCO thin-films and nanocomposites (thickness 150-200 nm) were grown at ICMAB on 5×5 mm^2 $LaAlO_3$ substrates using a metal–organic decomposition method based on the trifluoroacetate (TFA) route [51], [52]. YBCO and YBCO - BHO NP precursor films were deposited by spin coating. The coatings were pyrolyzed up to 310ºC in a humid O_2 atmosphere to form nanocrystalline precursor films. Subsequently, the films were crystallized at 810 °C in a wet N_2 atmosphere with an O_2

partial pressure of 200 ppm and oxygenated at 450 °C for 2 h in a dry oxygen atmosphere. For this study we considered a pristine CSD1 film with a nanostrain of ε = 0.1 % and effective anisotropy of γ_{eff} = 5, and two nanocomposites, CSD2 (with 12% mol. BHO, ε = 0.2 %, γ_{eff} = 2.5) and CSD3 (with 12% mol. BHO, ε = 0.25 %, γ_{eff} = 5), the later grown by a flash heating method. A detailed description of these type of CSD nanocomposites can be found in [34]. Transmission Electron Microscope (TEM) images of CSD nanocomposites showed a large amount of intergrowth for the nanocomposite samples, being shorter for CSD3 due to the flash heating growth [34]. Twin planes were also present in both pristine and nanocomposite CSD films, to a variable extend that depends on the nature and amount of nanoparticles [53],[54],[55].

PLD epitaxial *c*-axis oriented thin films were grown at ENEA on 7.5×7.5 mm^2 $SrTiO_3$ single crystal substrates. The thickness of the films, in the range 150 – 230 nm, was estimated by atomic force microscopy (AFM) and/or cross section TEM analysis. A XeCl excimer laser, with a radiation wavelength ν_L = 308 nm, was used for the films deposition, keeping the laser fluence at about 2 J/cm^2 and the laser repetition rate at f_L = 10 Hz. The growth temperatures were 850 °C and 840 °C for pristine and nanocomposite YBCO samples, respectively. The films studied in this work are a pristine reference YBCO sample PLD1 and two identical YBCO films with 5 % mol. BYNTO doping (PLD2 and PLD3). The doped films were deposited by using a mixed target of YBCO with the BYNTO secondary phase, with the ratio Nb : Ta = 1. Details in the target manufacturing process can be found in [19]. TEM cross section analysis revealed a well-defined BYNTO columnar growth in the YBCO matrix: continuous and splayed columns develop through the whole film starting from the film-substrate interface to the top of the film. The column density is $B_{eq} = n_{col} \Phi_0 \approx 5.2$ T [56]. In addition, the presence of a large number of Y_2O_3 nanoparticles in concurrence with the columns was observed [56].

Transport properties were measured using a four-probe configuration in 10–30 μm tracks, patterned in a 4-point configuration by optical lithography and subsequent wet chemical etching. Silver or gold contacts were sputtered allowing measurements of *I-V* characteristics. A voltage criterion of 5 μV cm^{-1} was used to obtain the critical current values. Angular dependent current density curves at different magnetic fields and temperatures, $J_c(\theta, H, T)$, were obtained for fields ranging from $\mu_0 H$ = 0–9 T at different current field orientations, θ = 0°–90° (with θ = 0° for *H*//c and 90° for *H*//ab) and temperatures ranging from 5-77 K.

Microwave measurements were performed in as-grown films with the dielectric-loaded resonator technique [57], [58] in order to gain access to the magnetic-field-induced variation of the surface impedance of superconducting YBCO thin-films. The thin-film is incorporated in the base of a cylindrical copper cavity loaded with a cylindrical sapphire single crystal. The structure resonates in the TE_{011} mode at ν = 47.3 GHz. We measure at fixed temperature *T* the magnetic field-induced change of the resonance shape of the resonator, whence [59] we derive the quality factor *Q* and the resonant frequency f_0 and finally the variation of the complex resistivity due to the vortex motion, according to [60]:

$$\rho_v(H) - \rho_v(0) = G t_s \left[\frac{1}{Q(H)} - \frac{1}{Q(0)} + 2\mathrm{i} \frac{f_0(H) - f_0(0)}{f_0(0)} \right] \quad , \quad [1]$$

where $\rho_v = \rho_{v1} + \mathrm{i}\, \rho_{v2}$ is the vortex motion complex resistivity (see Sec.3.2 later on), *G* is a calculated geometrical factor, and t_s is the film thickness. In Eq. [1] we have made use of the fact that the films are not thicker than a few London penetration depth [61], and that for the magnetic field range $\mu_0 H$ = 0-0.8 T employed there is no significant contribution to the response from the change in superfluid [62].

3. Results and Discussion

3.1 Transport critical current density measurements

Figure 1 shows the comparison of the critical current density as a function of magnetic field at *H*//c, for two pristine and nanocomposite samples grown by PLD (PLD1 and PLD2) and CSD (CSD1 and CSD2), at 77 K and 65 K. In a log-log representation the magnetic field dependence of all samples shows a plateu at low fields, associated to single vortex pinning, and a power-law behaviour at intermediate fields, with an exponent α associated to a collective pinning regime.

At higher fields, once the irrevestibility field is approached, J_c suffers a much faster decay. The transition from single vortex to collective pinning regimes is defined by the crossover field *H**, which has been determined at 90% of self-field J_c. The transition from the collective pinning regime to the fast decay associated to the irreversibity field has been defined as *H*', which was determined at 10% of self-field J_c.

Figure 1(a) shows the power law fittings obtained for all the samples, as dashed lines and, as an example, the crossover field H^* and H' obtained for PLD2.

Although, the J_c performance is improved for both PLD and CSD nanocomposites, the microstructure induced in the two samples produce different effects on the $J_c(H)$ curves. The self-field J_c is slightly decreased on PLD nanocomposites, provably associated to a cross-section reduction due to the presence on non-superconducting nano-rods. In the case of CSD, self-field J_c reduction due to cross section effects can be precluded up to large NP concentrations (>10-15% mol.) if segregation is avoided [39].

The most evident feature in the in-field performance of CSD nanocomposites is a smoother magnetic field decay of $J_c(H)$, with an extended single vortex plateau, i.e. shift of H^* up to higher fields. Contrary, for PLD nanocomposites the value of H^* barely changes and the most remarkable effect is a reduction of the power law exponent α and a strong increase of the irreversitility field.

In order to better compare the pinning effects for the two kinds of nanocomposites, we have plotted in Figure 2 the changes obtained in H^* and α when introducing BHO nanoparticles in CSD2 and BYNTO nanorods in PLD2. It is clear from the figure that the value of H^* is notably enhanced in the CSD nanocomposites at both 65 K and 77 K, while it remains roughly constant in the case of PLD nanocomposite. Regarding the power-law behaviour, large α values are obtained for the pristine CSD sample $\alpha \sim 0.7$ which are reduced to $\alpha \sim 0.5$ by adding nanoparticles. In the case of PLD samples, we have found an already lower value of α for the pristine sample, $\alpha \sim 0.4$, which is reduced to $\alpha \sim 0.3$ by adding nanorods. It is worth noticing that PLD $J_c(H)$ curves exhibit a smoother transition from single to collective vortex (identifiable by a power law with a well defined α exponent) regimes as can be observed in by the presence of a faster J_c decay in a narrow magnetic field interval for $\mu_0 H > \mu_0 H^*$. The origin of this feature has not deeply clarified.

At each temperature, the comparison of the critical current density curves $J_c(H)$ of the two nanocomposites reveals that CSD2 presents larger J_c at lower magnetic fields, whereas PLD2 has superior J_c above a certain intersection field, H_{int} (see arrows signalling H_{int}(65 K), H_{int}(77 K) in Figs. 1a and 1b, respectively). With the aim to compare the pinning performance of PLD and CSD nanocomposites we have built up a general H-T diagram in which we have plotted the three characteristic lines: $H^*(T)$, $H'(T)$ and $H_{int}(T)$, see Figure 3. The bands in the H-T diagram represent typical values determined through transport measurements at 5-77 K of a large number of samples at ICMAB and ENEA (the symbols correspond to the samples reported in Fig. 1a-b). As a general trend we observe that the single-to-collective pinning crossover field H^* is shifted to higher values, and presents a broader dispersion of values (depending on the particular sample microstructure) for the CSD nanocomposites. On the other hand, PLD nanocomposites exhibit larger $H'(T)$, which is associated to a higher irreversibility line. At intermediate magnetic fields, where pinning is dominated by a collective power-law regime PLD nanocomposites present better performance above a certain line $H_{int}(T)$ lying at ~1 T, whereas CSD nanocomposites show improved $J_c(H)$ behaviour below H_{int}.

The angular anisotropy of $J_c(\theta)$, i.e. its dependence with the orientation of the magnetic field, is a critial issue in may applications. For this purpose, it is desirable to have isotropic pinning defects, able to act in any field direction. The angular dependence of J_c of the four samples (CSD1,CSD2 and PLD1, PLD2) is shown in Figure 4. The pinning performance of the PLD nanocomposite with BYNTO nanorods shows a strong c-axis peak at intermediate-high fields (>1 T), when the magnetic field is aligned with the nanorods ($H//c$, $\theta = 180^o$), according to a very large enhancement of J_c observed at this orientation (see Figure 1). The CSD nanocomposite shows lower J_c values at H//c but with the benefit of having a flatter $J_c(\theta)$ dependence due to the presence of isotropic defects. As discussed above, improved J_c performances at any field orientation are obtained for the CSD nanocomposite at low fields (<1 T).

3.2 Microwave measurements

Microwave surface impedance measurements at different constant temperatures were performed in the pristine and nanocomposite PLD (PLD1 and PLD3) and CSD (CSD1, CSD3) films, at different magnetic fields applied with $H//c$. Figure 5 shows a schematic of the experimental resonator setup and, as an example, typical raw MW data as well as the derived complex resistivity for one of the samples (PLD3). The magnetic-field shift of the complex resistivity ρ_v is linked to the vortex motion parameters through the equation of motion of the vortex line [63], written in absence of thermal forces [64]:

$$\eta \boldsymbol{v} + \nabla U(\boldsymbol{x}) = \boldsymbol{J_{rf}} \times \Phi_0, \qquad [2]$$

where $\boldsymbol{J_{rf}}$ is the microwave current density, η is the vortex viscosity and U is the pinning potential. At high oscillating frequencies $\omega/2\pi$, the vortex experiences a tiny displacement $\boldsymbol{x}$ from its equilibrium position so that one can approximate:

$$\nabla U(\boldsymbol{x}) \simeq k_p \boldsymbol{x}, \qquad [3]$$

which defines the *pinning constant* (or *Labusch parameter*) k_p, representing the elastic recall on the vortex toward the pinning center. We stress that the vortex dynamics at high frequencies is very different from the dc case: vortices oscillate for a tiny fraction of their intervortex spacing. Thus, microwaves probe the very short displacement dynamics. As such, significant signal can be detected even deep in the vortex solid phase. Moreover, due to the very small oscillations, it is safe to make use of Eq. [2] which is a single-vortex equation: all the complex interactions between vortices and pinning centers result in a certain spatial vortex configuration which contributes little to the dynamics, being the latter determined by very small oscillations around the vortex equilibrium [65].
From Eq. [2] one derives the vortex motion resistivity [64]:

$$\rho_{v1} + \mathrm{i}\rho_{v2} = \frac{\Phi_0 B}{\eta} \frac{1}{1 - \mathrm{i}k_p/\eta\nu} \quad . \qquad [4]$$

Thus, from measurements of ρ_{v1} and ρ_{v2} one directly obtains the vortex parameters (the possible role of thermal effects has been discussed extensively in [63]). On a technical ground, we note that the numerical inversion from the data produces a very large scattering at low fields, so that the data below 50 mT are omitted.

In this paper we focus on the pinning properties, and thus on k_p. Eq. [3] clearly shows that k_p is a measure of the *steepness* of the pinning potential. This is an important feature in the discussion of the data. A second important point comes from Eq. [2] being a single-vortex equation. Thus, the measured response of the overall system of many vortices, when interpreted with Eq. [4], should be understood as an average over all vortices. As such, the number of pinning centers affects the average k_p: more pinned vortices imply a larger average k_p.

For what concerns the magnetic field dependence, a decreasing $k_p(H)$ has been attributed to incipient collective pinning due to fluxon softening [66]. As we will see, this is a feature common to all films but the PLD nanocomposite.

We then derived the (average) pinning constant as a function of the field, $k_p(H)$, at different temperatures between 67-83.5 K in the low-field regime below 1 T, in CSD and PLD samples. Figure 6 summarises the $k_p(H)$ field-dependence at several constant T determined for the CSD (Fig. 6a) and PLD-grown (Fig. 6b) pristine films and nanocomposites. Several features emerge: (i) nanodefects increase the absolute value of k_p, (ii) k_p attains larger values in PLD samples, and (iii) in nanocomposite PLD and CSD the field dependence is different.

In both cases it is observed that at each temperature and field investigated, the addition of nanodefects has the effect to significantly increase the pinning constant. Looking at the CSD samples, two features emerge. First, at same (or close) temperatures, the low-field k_p for the pristine and NC samples are similar. Second, with increasing the magnetic field, the $k_p(H)$ dependencies of pristine and nanocomposite films are similar, with an immediate decrease of k_p with increasing field, the only difference being the larger value of k_p in the nanocomposite. These features are consistent with a pinning effect mainly due to a larger number of pinning centres in nanocomposites. A second effect that cannot be excluded is an increased steepness of the additional pinning centres with respect to those existing in the pristine film. It is remarkable that this effect takes place on the scale of the amplitude of the vortex oscillations, ~0.1 nm. However, the similar field-dependence in pristine and nanocomposite points to the same qualitative pinning regime in the low-field region. This behaviour is common to other chemically-grown YBCO nanocomposites [67]. As mentioned before, a decreasing $k_p(H)$ is a manifestation of fluxon softening, with a drive toward collective pinning. Since measurements are taken deep in the vortex solid phase, with the microwave probe we can observe the transformation toward collective pinning even in the vortex solid phase. The addition of NPs, which induces an increase of the YBCO isotropic nanostrain, leads to a k_p(H) dependence smoother but qualitatively similar than in pristine films, indicating that the physics of vortex pinning is unchanged.

PLD films (Fig. 6b) exhibit instead significant differences with respect to CSD films: the low-field limit of k_p is different in pristine and nanocomposites, the absolute values of k_p are larger, the increase of k_p with nanostructuring is larger and, most important, the field dependence changes dramatically with the

This article has been accepted for publication in IOP-Superconductor Science and Technology. This is the author's version which has not been fully edited and content may change prior to final publication.
Citation information: DOI 10.1088/1361-6668/ab8f18

introduction of nanorods. From all these features one can state that steeper pinning centres are introduced with nanorods, so that vortices pinned by nanorods do not undergo a significant softening.

The quantitative effect of NPs and nanorods is reported in Fig. 7, where we report $k_p(T)$ measured at $\mu_0 H$=0.5 T. There, the strong increase in PLD samples with nanorods is evident. In PLD samples, nanorods increase k_p by a factor of ~4, while NPs in CSD samples produce a smaller increase, by a factor ~2. This is not surprising: nanorods are in fact expected to be very efficient in vortex pinning, especially when the field is aligned (or approximately aligned) with the nanorods, as in this case.

Bearing in mind Eqs. [2,3], the large increase of k_p with the introduction of nanorods hints to a steepening of the pinning potential or, analogously, that existing defects (e.g. twin planes) determine a much broader pinning potential than nanorods. However, the most important feature is that the magnetic-field dependence of k_p remains flat or even slightly increasing in films with nanorods. This behaviour was already observed in YBCO/BZO PLD films [48,68,69] and, as opposed to the decrease of $k_p(H)$, points to pinning of rigid fluxons, thanks to the 1D nature of nanorods. Nanorods change the qualitative nature of fluxon pinning, as observed in the short-vortex-displacement (small oscillation) regime: the rigid vortex pinning extends to higher fields, since nanorods hinder the fluxon softening in a significant fraction of the fluxons. In fact, in PLD YBCO/BZO (with nanorods), by comparing the angular dependence of the microwave response and of J_c [48], it was shown that rigidly pinned fluxons produce a caging effect on other, possibly softer, fluxons that are not rigidly pinned by nanorods. As a consequence, J_c is enhanced more than the enhancement of k_p. In this context, the depinning of flux lines (that gives rise to J_c) can be dominated by the softer pinned vortices. In order to reinforce this speculation, we remind that increasing the density of nanorods in YBCO/BZO increased the field range of constant k_p [70], pointing to a change of regime from soft to rigid vortices with increasing the nanorods density.

The very different effect of NPs and nanorods on the high-frequency dynamics is exemplified in Fig. 8, where we report the data for all four samples at the same temperature T~77 K. As it can be seen, only the PLD sample with nanorods exhibits an almost field-independent $k_p(H)$, consistently with the absence of softening due to the presence of elongated, 1D pinning centres.

5. Conclusions

The vortex pinning response in dc and at 50 GHz of YBCO nanocomposites with different types of defects, BYNTO nanorods in PLD films and BHO nanoparticles in CSD films, was characterised combining transport and microwave surface impedance measurements. Transport critical current density measurements allowed us to draw an *H-T* diagram with different characteristic fields to compare the two types of nanocomposites at *H*//*c*. Whereas CSD NCs exhibit a higher single-to-collective $H^*(T)$ line, PLD NCs present larger irreversibility fields. As a consequence, CSD NCs have superior performances a lower fields, < 1 T, above which the PLD nanocomposites take over.

Microwave results demonstrate that nanodefects increase the pinning constant k_p in both types of nanocomposites, although the effects on the field-dependence are qualitatively different. For CSD NCs, where the addition of nanoparticles induces an increase of the YBCO isotropic nanostrain, an improvement of the $k_p(H)$ dependence is observed, qualitatively similar but with a smoother decay than that of pristine samples. In contrast, for PLD NCs, the introduction of 1D nanorods produces an extension of the rigid vortex pinning to higher fields, leading to an increasing $k_p(H)$ curve, instead of the decreasing curve observed for pristine samples.

Our investigation of the in-field pinning efficiency of defects of different dimensionality defects at different frequency ranges provides useful guidelines to select the best material under the different operating conditions required for applications.

Acknowledgements

This work has been carried out within the framework of the EUROfusion Consortium and has received funding from the Euratom Research and Training Programme 2014-2018 and 2019-2020 under grant agreement No 633053. The views and opinions expressed herein do not necessarily reflect those of the European Commission. We acknowledge financial support from Spanish Ministry of Economy and Competitiveness through the Severo Ochoa Programme for Centres of Excellence in R&D (SEV-2015-0496), SUMATE project RTI2018-095853-B-C21, cofinanced by the European Regional Development Fund, COST-Nanocohybri CA16218, DWARFS project (MAT2017-83468-R) and Catalan Government with 2017-SGR-1519 and XRE4S.

This article has been accepted for publication in IOP-Superconductor Science and Technology. This is the author's version which has not been fully edited and content may change prior to final publication.
Citation information: DOI 10.1088/1361-6668/ab8f18

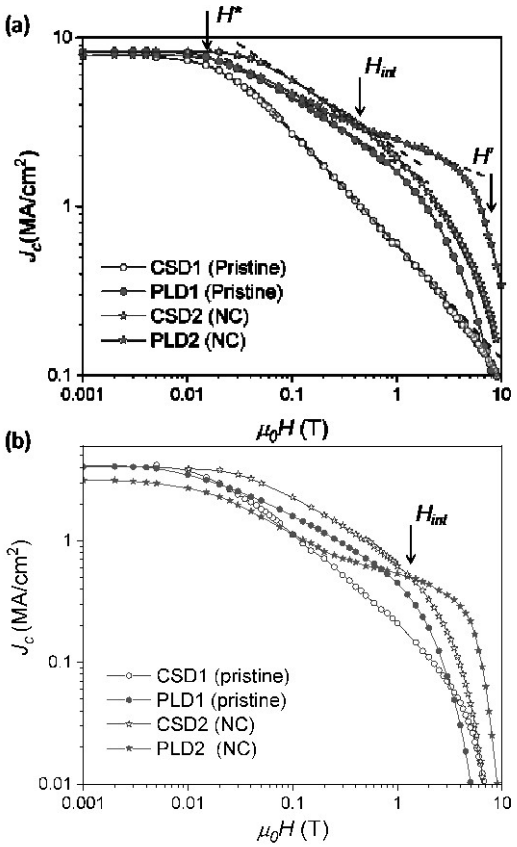

Figure 1. Magnetic field dependence of the critical current density obtained at $H//c$, for pristine and nanocomposite YBCO films grown by CSD and PLD at (a) 65 K (the arrows signal the crossover fields H^* and H' for PLD2), and (b) 77 K. Dashed lines in (a) are power-law fits. At each temperature, the intersection field at which the $J_c(H)$ curves for the PLD2 and CSD2 curves cross, $H_{int}(T)$ is signaled.

This article has been accepted for publication in IOP-Superconductor Science and Technology. This is the author's version which has not been fully edited and content may change prior to final publication.
Citation information: DOI 10.1088/1361-6668/ab8f18

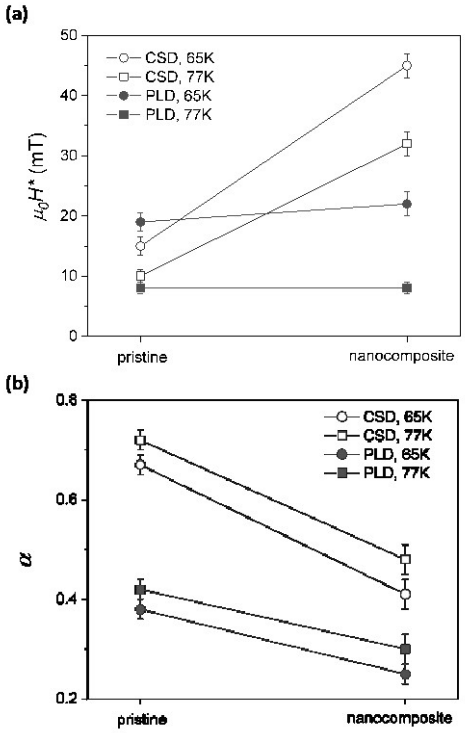

Figure 2. Values of (a) H^* and (b) α obtained for different nanocomposites (CSD1, CSD2; PLD1, PLD2) analized at 65 K and 77 K.

This article has been accepted for publication in IOP-Superconductor Science and Technology. This is the author's version which has not been fully edited and content may change prior to final publication.
Citation information: DOI 10.1088/1361-6668/ab8f18

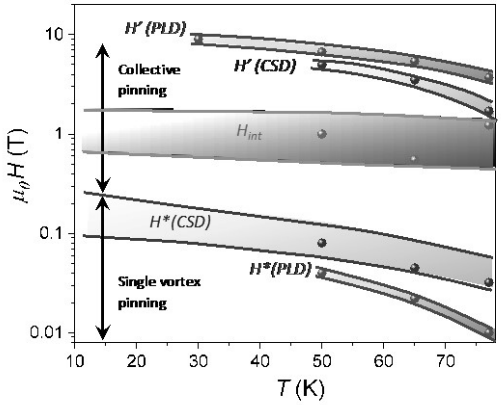

Figure 3. *H-T* diagram showing the magnetic fields *H**, *H'* and H_{int} (the field at which the J_c of the PLD nanocomposite is higher than that of the CSD one), at *H*//*c*. The symbols correspond to the samples CSD2 and PLD2 shown in Figure 1; the bands represent typical values measured for a larger number of sample at ICMAB and ENEA over the temperature range 5-77 K.

This article has been accepted for publication in IOP-Superconductor Science and Technology. This is the author's version which has not been fully edited and content may change prior to final publication.
Citation information: DOI 10.1088/1361-6668/ab8f18

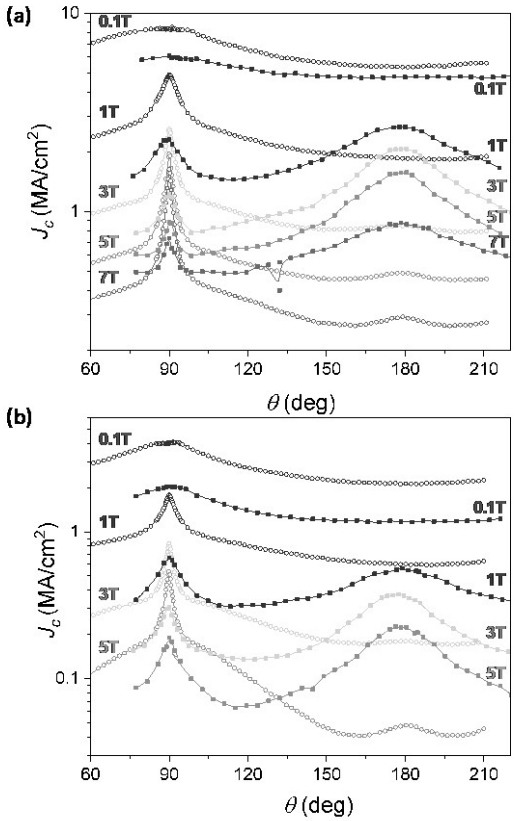

Figure 4. Angular dependence of the critical current density at (a) 65 K and (b) 77 K for YBCO-BHO CSD2 nanocomposite (open symbols) and YBCO-BYNTO PLD2 nanocompostie (closed symbols), at different magnetic fields.

This article has been accepted for publication in IOP-Superconductor Science and Technology. This is the author's version which has not been fully edited and content may change prior to final publication.
Citation information: DOI 10.1088/1361-6668/ab8f18

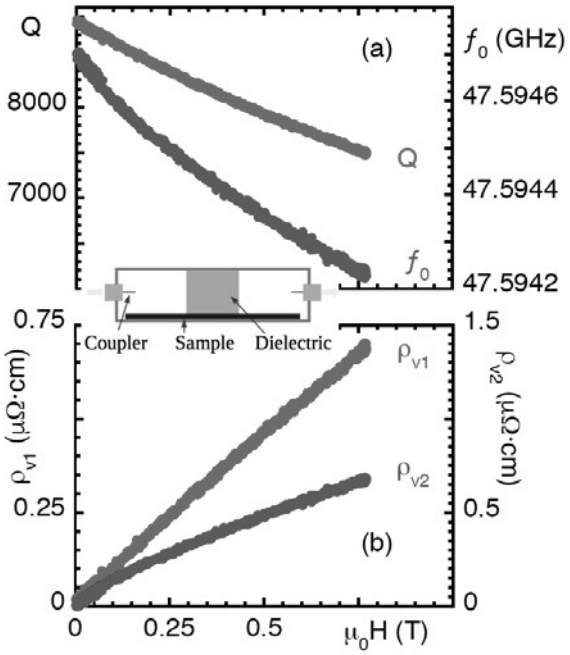

Figure 5. (a) Magnetic field dependence of the quality factor Q and resonance frequency f_0 for the YBCO PLD3 thin-film. (b) real and imaginary part of the complex resistivity derived from the data in (a) and Eq. [1]. Inset: sketch of the resonator.

This article has been accepted for publication in IOP-Superconductor Science and Technology. This is the author's version which has not been fully edited and content may change prior to final publication.
Citation information: DOI 10.1088/1361-6668/ab8f18

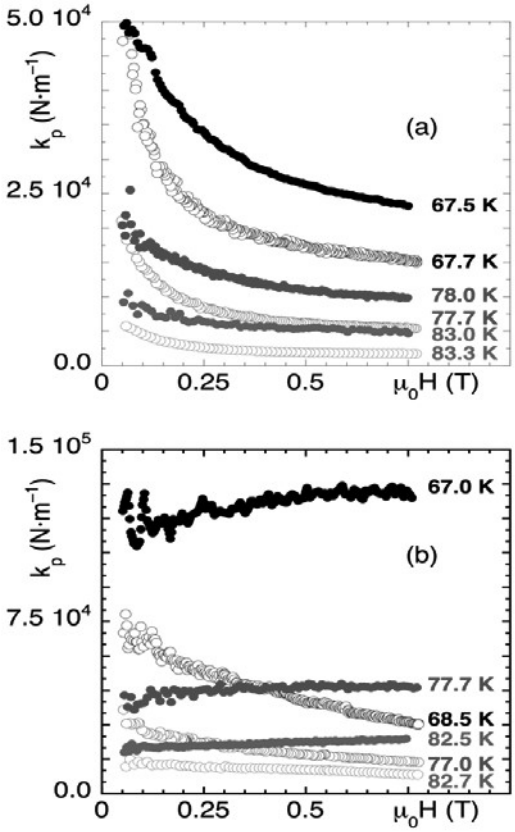

Figure 6. Pinning constant (k_p) as a function of the applied magnetic field *H*//c, at different constant temperatures for (a) CSD-pristine film CSD1 (open symbols) and nanocomposite with NPs, CSD3 (full symbols) samples, and (b) PLD-pristine film PLD1 (open symbols) and nancomposite with nanorods PLD3 (full symbols).

This article has been accepted for publication in IOP-Superconductor Science and Technology. This is the author's version which has not been fully edited and content may change prior to final publication.
Citation information: DOI 10.1088/1361-6668/ab8f18

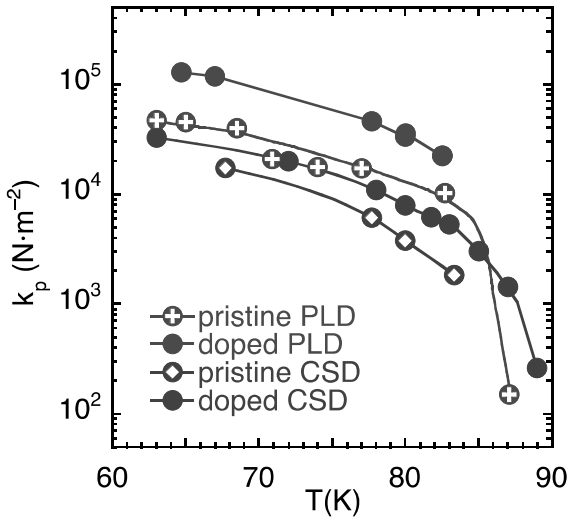

Figure 7. Pinning constant (k_p) as a function of the temperature at a fixed applied magnetic field $\mu_0 H$ = 0.5 T, in PLD films (purple symbols, PLD1 and PLD3) and CSD films (grey symbols, CSD1 and CSD3), pristine film (open symbols) and nanocomposite (full symbols).

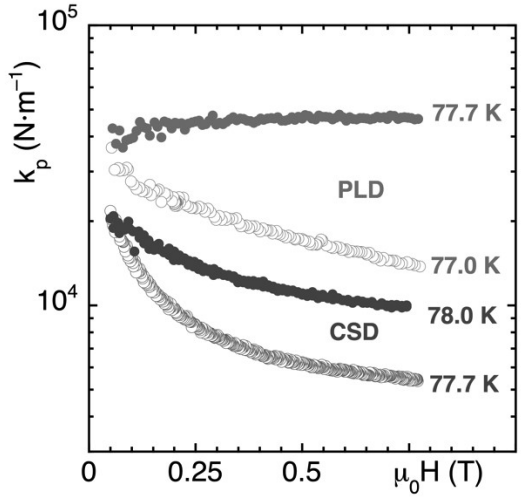

Figure 8. Pinning constant (k_p) as a function of the applied magnetic field *H*//*c*, at 77 K for investigated films: PLD samples PLD1, PLD3 (purple symbols) and CSD samples CSD1, CSD3 (grey symbols). Open symbols: pristine films; Bold symbols: nanocomposites.

References

[1] Larbalestier D, Gurevich A, Matthew Feldmann D and Polyanskii A 2010 High-Tcsuperconducting materials for electric power applications *Materials for Sustainable Energy: A Collection of Peer-Reviewed Research and Review Articles from Nature Publishing Group* ed V Dusastre (Nature Publishing Group) p 360

[2] Kang S, Goyal A, Li J, Gapud A A, Martin P M, Heatherly L, Thompson J R, Christen D K, List F A, Paranthaman M and Lee D F 2006 High-performance high-Tc superconducting wires *Science (80-.).* **311** 1911–1914

[3] MacManus-Driscoll J L, Foltyn S R, Jia Q X, Wang H, Serquis A, Civale L, Maiorov B, Hawley M E, Maley M P and Peterson D . 2004 Strongly enhanced current densities in superconducting coated conductors of YBa2Cu3O7–x + BaZrO3 *Nat. Mater.* **3** 439

[4] Mele P, Prassides K, Tarantini C, Palau A, Badica P, Jha A K and Endo T (Eds. . 2019 *Superconductivity: From Materials Science to Practical Applications* (Springer Nature Switzerland)

[5] Foltyn S R, Civale L, Macmanus-Driscoll J L, Jia Q X, Maiorov B, Wang H and Maley M 2007 Materials science challenges for high-temperature superconducting wire *Nat. Mater.* **6** 631–642

[6] Padamsee H 2001 The science and technology of superconducting cavities for accelerators *Supercond. Sci. Technol.* **14** R28R51

[7] Di Gioacchino D, Gatti C, Alesini D, Ligi C, Tocci S, Rettaroli A, Carugno G, Crescini N, Ruoso G, Braggio C, Falferi P, Gallo C S, Gambardella U, Iannone G, Lamanna G, Lombardi A, Mezzena R, Ortolan A, Pengo R, Silva E and Pompeo N 2019 Microwave Losses in a DC Magnetic Field in Superconducting Cavities for Axion Studies *IEEE Trans. Appl. Supercond.* **29** 3500605

[8] Calatroni S 2016 HTS Coatings for Impedance Reduction in Particle Accelerators: Case Study for the FCC at CERN *IEEE Trans. Appl. Supercond.* **3** 3500204

[9] Puig T, Krkotic P, Romanov A, O'Callaghan J, Zanin D, Neupert H, Pinto P, Demolon P, Costa A, Taborelli M, Perez F, Pont M, Gutierrez J and Calatroni S 2019 Coated conductor technology for the beamscreen chamber of future high energy circular colliders *Supercond. Sci. Technol.* **32** 094006–14

[10] Tavian L J 2014 Cryogenics Future Circular Collider Study Kickoff Meeting *Univ. Geneva, Switz. [online]*

[11] MacManus-Driscoll J L, MacManus-Driscoll J L, Zerrer P, Zerrer P, Wang H, Wang H, Yang H, Yang H, Yoon J, Yoon J, Fouchet A, Fouchet A, Yu R, Yu R, Blamire M G, Blamire M G, Jia Q and Jia Q 2008 Strain control and spontaneous phase ordering in vertical nanocomposite heteroepitaxial thin films. *Nat. Mater.* **7** 314–20

[12] Maiorov B, Baily S a, Zhou H, Ugurlu O, Kennison J a, Dowden P C, Holesinger T G, Foltyn S R and Civale L 2009 Synergetic combination of different types of defect to optimize pinning landscape using BaZrO3-doped YBa2Cu3O7 *Nat. Mater.* **8** 398–404

[13] Matsumoto K and Mele P 2010 Artificial pinning center technology to enhance vortex pinning in YBCO

coated conductors *Supercond. Sci. Technol.* **23** 014001

[14] Selvamanickam V, Chen Y, Shi T, Liu Y, Khatri N D, Liu J, Yao Y, Xiong X, Lei C and Soloveichik S 2013 Enhanced critical currents in (Gd,Y)Ba2Cu3Ox superconducting tapes with high levels of Zr addition *Supercond. Sci. Technol.* **26** 035006

[15] Llordes A, Palau A, Gazquez J, Coll M, Vlad R, Pomar A, Arbiol J, Guzman R, Ye S, Rouco V, Sandiumenge F, Ricart S, Puig T, Varela M, Chateigner D, Vanaken J, Gutierrez J, Morshchalkov V, Deutscher G, Magen C and Obradors X 2012 Nanoscale strain-induced pair suppression as a vortex-pinning mechanism in high-temperature superconductors *Nat. Mater.* **11** 329–36

[16] Gutiérrez J, Llordés A, Gázquez J, Gibert M, Romà N, Ricart S, Pomar A, Sandiumenge F, Mestres N, Puig T and Obradors X 2007 Strong isotropic flux pinning in solution-derived YBa2Cu3O7-x nanocomposite superconductor films. *Nat. Mater.* **6** 367–73

[17] Chen A, Weigand M, Bi Z, Zhang W, Lü X, Dowden P, Macmanus-Driscoll J L, Wang H and Jia Q 2014 Evolution of microstructure, strain and physical properties in oxide nanocomposite films *Sci. Rep.* **4** 5426

[18] Jha A K, Matsumoto K, Horide T, Saini S, Mele P, Yoshida Y and Awaji S 2014 Tuning the microstructure and vortex pinning properties of YBCO-based superconducting nanocomposite films by controlling the target rotation speed *Supercond. Sci. Technol.* **27** 025009–19

[19] Rizzo F, Augieri A, Angrisani Armenio A, Galluzzi V, Mancini A, Pinto V, Rufoloni A, Vannozzi A, Bianchetti M, Kursumovic A, MacManus-Driscoll J L, Meledin A, Van Tendeloo G and Celentano G 2016 Enhanced 77 K vortex-pinning in y Ba2Cu3O7-x films with Ba2Y TaO6 and mixed Ba2Y TaO6 + Ba2Y NbO6 nano-columnar inclusions with irreversibility field to 11 T *APL Mater.* **4** 061101–7

[20] Opherden L, Sieger M, Pahlke P, Huhne R, Schultz L, Meledin A, Van Tendeloo G, Nast R, Holzapfel B, Bianchetti M, MacManus-Driscoll J L and Hanisch J 2016 Large pinning forces and matching effects in YBa2Cu3O7-δ thin films with Ba2Y(Nb/Ta)O6 nano-precipitates *Sci. Rep.* **6** 21188–98

[21] Roma N, Morlens S, Ricart S, Zalamova K, Moreto J M, Pomar A, Puig T and Obradors X 2006 Acid anhydrides: A simple route to highly pure organometallic solutions for superconducting films *Supercond. Sci. Technol.* **19** 521–7

[22] Coll M, Gázquez J, Hühne R, Holzapfel B, Morilla Y, García-López J, Pomar A, Sandiumenge F, Puig T and Obradors X 2009 All chemical YBa2Cu307 superconducting multilayers: Critical role of CeO2 cap layer flatness *J. Mater. Res.* **24** 1446–54

[23] Vlad V R, Zalamova K, Coll M, Pomar A, Palau A and Gutierrez J 2009 Growth of Chemical Solution Deposited TFAYBCO/MOD(Ce, Zr)O2/ABADYSZ/SS Coated Conductors *IEEE Trans. Appl. Supercond.* **19** 3212–3215

[24] Rupich M W, Li X, Thieme C, Sathyamurthy S, Fleshler S, Tucker D, Thompson E, Schreiber J, Lynch J, Buczek D, Demoranville K, Inch J, Cedrone P and Slack J 2010 Advances in second generation high temperature superconducting wire manufacturing and R&D at American Superconductor Corporation *Supercond. Sci. Technol.* **23** 014015–24

[25] Izumi T and Nakaoka K 2018 Control of artificial pinning centers in REBCO coated conductors derived from the trifluoroacetate metal-organic deposition process *Supercond. Sci. Technol.* **31** 034008

[26] Coll M, Guzman R, Garcés P, Gazquez J, Rouco V, Palau A, Ye S, Magen C, Suo H, Castro H, Puig T and Obradors X 2014 Size-controlled spontaneously segregated Ba2YTaO6 nanoparticles in YBa2Cu3O7 nanocomposites obtained by chemical solution deposition *Supercond. Sci. Technol.* **27** 044008

[27] Ye S, Suo H, Wu Z, Liu M, Xu Y, Ma L and Zhou M 2011 Preparation of solution-based YBCO films with BaSnO3 particles *Phys. C Supercond. its Appl.* **471** 265–9

[28] Selvamanickam V, Gharahcheshmeh M H, Xu A, Zhang Y and Galstyan E 2015 Requirements to achieve high in-field critical current density at 30 K in heavily-doped (Gd,Y)Ba2Cu3Oxsuperconductor tapes *Supercond. Sci. Technol.* **28** 4–9

[29] Gutiérrez J, Llordés A, Gázquez J, Gibert M, Romà N, Ricart S, Pomar A, Sandiumenge F, Mestres N, Puig T and Obradors X 2007 Strong isotropic flux pinning in solution-derived YBa 2Cu 3O7-x nanocomposite superconductor films *Nat. Mater.* **6** 367–73

[30] Martínez-Julián F, Ricart S, Pomar A, Coll M, Abellán P, Sandiumenge F, Casanove M J, Obradors X, Puig T, Pastoriza-Santos I and Liz-Marzán L M 2011 Chemical solution approaches to YBa2Cu3O 7-δ-au nanocomposite superconducting thin films *J. Nanosci. Nanotechnol.* **11** 3245–55

[31] Bretos I, Schneller T, Falter M, Bäcker M, Hollmann E, Wördenweber R, Leopoldo Molina-Luna de G V T and Eiblf O 2015 Solution-derived YBa2Cu3O7−δ (YBCO) superconducting films with BaZrO3 (BZO) nanodots based on reverse micelle stabilized nanoparticles *J. Mater. Chem. C* **3** 3979

[32] Cayado P, De Keukeleere K, Garzón A, Perez-Mirabet L, Meledin A, De Roo J, Vallés F, Mundet B, Rijckaert H, Pollefeyt G, Coll M, Ricart S, Palau A, Gázquez J, Ros J, Van Tendeloo G, Van Driessche I, Puig T and Obradors X 2015 Epitaxial YBa2Cu3O7-x nanocomposite thin films from colloidal solutions *Supercond. Sci. Technol.* **28** 124007

[33] De Keukeleere K, Cayado P, Meledin A, Vallès F, De Roo J, Rijckaert H, Pollefeyt G, Bruneel E, Palau A, Coll M, Ricart S, Van Tendeloo G, Puig T, Obradors X and Van Driessche I 2016 Superconducting YBa2Cu3O7–δ Nanocomposites Using Preformed ZrO2 Nanocrystals: Growth Mechanisms and Vortex Pinning Properties *Adv. Electron. Mater.* **2** 1–9

[34] Li Z, Coll M, Mundet B, Chamorro N, Vallès F, Palau A, Gazquez J, Ricart S, Puig T and Obradors X 2019 Control of nanostructure and pinning properties in solution deposited YBa 2 Cu 3 O 7−x nanocomposites with preformed perovskite nanoparticles *Sci. Rep.* **9** 5828

[35] Obradors X, Puig T, Li Z, Pop C, Mundet B, Chamorro N, Vallés F, Coll M, Ricart S, Vallejo B, Pino F,

Palau A, Gázquez J, Ros J and Usoskin A 2018 Epitaxial YBa 2 Cu 3 O 7-x nanocomposite films and coated conductors from BaMO 3 (M = Zr, Hf) colloidal solutions *Supercond. Sci. Technol.* **31** 044001

[36] Guzmán R, Gázquez J, Mundet B, Coll M, Obradors X and Puig T 2017 Probing localized strain in solution-derived YBa2Cu3O7−δ nanocomposite thin films *Phys. Rev. Mater.* **1** 024801

[37] Palau A, Bartolomé E, Llordés A, Puig T and Obradors X 2011 Isotropic and anisotropic pinning in TFA-grown YBa2Cu 3O7 - X films with BaZrO3 nanoparticles *Supercond. Sci. Technol.* **24** 125010

[38] Rouco V, Bartolomé E, Palau a, Coll M, Obradors X and Puig T 2012 Nanostrain induced pinning in YBa 2 Cu 3 O 7− x nanocomposites even close to the irreversibility line *Supercond. Sci. Technol.* **25** 122001

[39] Palau A, Valles F, Rouco V, Coll M, Li Z, Pop C, Mundet B, Gazquez J, Guzman R, Gutierrez J, Obradors X and Puig T 2018 Disentangling vortex pinning landscape in chemical solution deposited superconducting YBa2Cu3O7-x films and nanocomposites *Supercond. Sci. Technol.* **31** 034004

[40] Ivan I, Ionescu A M, Sandu V, Crisan A and Miu L 2018 Vortex dynamics driven by AC magnetic field in YBCO thin films with complex pinning structures *Supercond. Sci. Technol.* **31** 105012

[41] Bartolomé E, Palau A, Llordés A, Puig T and Obradors X 2010 Vortex dynamics at high ac amplitudes of trifluoracetate route grown YBa2Cu3O7-x-BaZrO3 nanocomposites *Phys. Rev. B* **81** 184530

[42] Bartolomé E, Palau A, Llordés A, Puig T and Obradors X 2010 Vortex oscillations in TFA-grown YBCO thin-films with BZO nanoparticles *Phys. C Supercond. its Appl.* **470** 2033–9

[43] Torokhtii K, Pompeo N, Rizzo F, Augieri A, Celentano G, Mancini A and Silva E 2016 Measurement of Vortex Pinning in YBCO and YBCO/BZO Coated Conductors Using a Microwave Technique *IEEE Trans. Appl. Supercond.* **26** 8001605

[44] Frolova A, Pompeo N, Rizzo F, Torokhtii K, Augieri A, Galluzzi V, Mancini A, Vannozzi A, Rufoloni A, Celentano G and Silva E 2018 Critical current and vortex pinning properties in YBa2Cu3O7-x films with Ba2YTaO6 + Ba2YNbO6 and BaZrO3 nanoinclusions by DC transport and microwave measurements *IEEE Trans. Appl. Supercond.* **28** 7500805

[45] Pompeo N, Torokhtii K, Augieri A, Celentano G, Galluzzi V and Silva E 2014 Directional pinning and anisotropy in YBa2Cu3O 7-x with BaZrO3 nanorods: Intrinsic and nanorods-induced anisotropy *Phys. C Supercond. its Appl.* **503** 146–9

[46] Pompeo N, Torokhtii K, Alimenti A, Mancini A, Celentano G and Silva E 2019 Vortex Pinning and Flux Flow Microwave Studies of Coated Conductors *IEEE Trans. Appl. Supercond.* **29** 8003405

[47] Pompeo N, Torokhtii K and Silva E 2018 Extraction of the complex resistivity and pinning parameters from microwave surface impedance measurements of coated conductors *IEEE Trans. Appl. Supercond.* **28** 9000505

[48] Pompeo N, Augieri A, Torokhtii K, Galluzzi V, Celentano G and Silva E 2013 Anisotropy and directional pinning in YBa2Cu3O 7-x with BaZrO3 nanorods *Appl. Phys. Lett.* **103** 022603

[49] Bartolomé E, Vallés F, Palau A, Rouco V, Pompeo N, Balakirev F F, Maiorov B, Civale L, Puig T, Obradors X and Silva E 2019 Intrinsic anisotropy versus effective pinning anisotropy in YBa2Cu3O7 thin films and nanocomposites *Phys. Rev. B* **100** 1–9

[50] Pompeo N, Alimenti A, Torokhtii K, Bartolome E, Palau A, Puig T, Augieri A, Galluzzi V, Mancini A, Celentano G, Obradors X and Silva E 2019 Intrinsic anisotropy and pinning anisotropy in nanostructured YBCO from microwave measurements *Supercond. Sci. Technol.* accepted, in press

[51] Palmer X, Pop C, Eloussifi H, Villarejo B, Roura P, Farjas J, Calleja A, Palau A, Obradors X, Puig T and Ricart S 2016 Solution design for low-fluorine trifluoroacetate route to YBa2Cu3O7 films *Supercond. Sci. Technol.* **29** 24002

[52] Obradors X, Puig T, Ricart S, Coll M, Gazquez J, Palau a and Granados X 2012 Growth, nanostructure and vortex pinning in superconducting YBa 2 Cu 3 O 7 thin films based on trifluoroacetate solutions *Supercond. Sci. Technol.* **25** 123001

[53] Rouco V, Palau A, Guzman R, Gazquez J, Coll M, Obradors X and Puig T 2014 Role of twin boundaries on vortex pinning of CSD YBCO nanocomposites *Supercond. Sci. Technol.* **27** 125009

[54] Palau A, Durrell J H, MacManus-Driscoll J L, Harrington S, Puig T, Sandiumenge F, Obradors X and Blamire M G 2006 Crossover between channeling and pinning at twin boundaries in YBa2Cu3O7 thin films *Phys. Rev. Lett.* **97** 257002

[55] Guzman R, Gazquez J, Rouco V, Palau a., Magen C, Varela M, Arbiol J, Obradors X and Puig T 2013 Strain-driven broken twin boundary coherence in YBa2Cu3O7−δ nanocomposite thin films *Appl. Phys. Lett.* **102** 081906

[56] Rizzo F, Augieri A, Kursumovic A, Bianchetti M, Opherden L, Sieger M, Hühne R, Hänisch J, Meledin A, Van Tendeloo G, Macmanus-Driscoll J L and Celentano G 2018 Pushing the limits of applicability of REBCO coated conductor films through fine chemical tuning and nanoengineering of inclusions *Nanoscale* **10** 8187–95

[57] Pompeo N, Torokhtii K and Silva E 2014 Dielectric resonators for the Measurements of the Surface Impedence of Superconducting Films *Meas. Sci. Rev.* **14** 64 – 170

[58] Alimenti A, Torokhtii K, Silva E and Pompeo N 2019 Challenging microwave resonant measurement techniques for conducting material characterization *Meas. Sci. Technol. 30* **30** 065601

[59] Pompeo N, Torokhtii K, Leccese F, Scorza A, Sciuto S and Silva E 2017 Fitting strategy of resonance curves from microwave resonators with non-idealities, in *Proceedings of the IEEE International Instrumentation and Measurement Technology Conference (I2MTC)* (Turin, Italy)

[60] Chen L F, Ong C K, Neo C P, Varadan V V and Varadan V K 2004 *Microwave Electronics: Measurement and Materials Characterization*

[61] Pompeo N, Torokhtii K and Silva E 2017 Substrate and finite-thickness-induced uncertainties in surface impedance measurements of thin conducting film *Proceedings of the IEEE International Instrumentation and Measurement Technology Conference (I2MTC)* (Torino)

[62] Coffey M W and Clem J R 1992 Theory of high-frequency linear response of isotropic type-II superconductors in the mixed state *Phys. Rev. B* **46** 11757–64

[63] Pompeo N and Silva E 2008 Reliable determination of vortex parameters from measurements of the microwave complex resistivity *Phys. Rev. B - Condens. Matter Mater. Phys.* **78** 1–10

[64] Gittleman J I and Rosenblum B 1966 No Title *Phys. Rev. Lett.* **16** 734

[65] Tomasch W J, Blackstead H A, Ruggiero S T, McGinn P J, Clem J R, Shen K, Weber J W and Boyne D 1988 Magnetic field dependence of nonresonant microwave power dissipation in YBa2Cu3O7-x *Phys. Rev. B* **37** 9864

[66] Golosovsky M, Tsindlekht M and Davidov D 1996 High-frequency vortex dynamics in YBaCuO *Supercond. Sci. Technol.* **9** 1–15

[67] Torokhtii K, Pompeo N, Frolova A, Pinto V, Angrisani Armenio A, Piperno L, Celentano G, Petrisor T, Ciontea L, Mos R B, Nasui M, Sotgiu G and Silva E 2017 Microwave Measurements of Pinning Properties in Chemically Deposited YBCO/BZO Films *IEEE Trans. Appl. Supercond.* **27** 8000405

[68] Pompeo N, Rogai R, Silva E, Augieri A, Galluzzi V and Celentano G 2007 Reduction of the field-dependent microwave surface resistance in YBa 2 Cu 3 O 7 − δ with sub-micrometric BaZrO 3 inclusions as a function of BaZrO 3 concentration . *Appl. Phys. Lett.* **91** 182507

[69] Augieri A, Celentano G, Galluzzi V, Mancini A, Rufoloni A, Vannozzi A, Armenio A A, Petrisor T, Ciontea L, Rubanov S, Silva E and Pompeo N 2010 Pinning analyses on epitaxial YBa2Cu3O7-d films with BaZrO3 inclusions *J. Appl. Phys.* **108** 063906

[70] Silva E, Pompeo N, Rogai R, Augieri A and Galluzzi V 2010 Effect of nanosize BaZrO3 inclusions on vortex parameters in YBa2Cu3O7−x *J. Phys. Conf. Ser.* **234** 012040